Seismic risk and loss assessment for Kalamata (SW Peloponnese, Greece) from neighbouring shallow sources

I. Kassaras[1], D. Kazantzidou-Firtinidou[1], A. Ganas[2], V. Kapetanidis[1], C. Tsimi[2], S. Valkaniotis[3], N. Sakellariou[1] and S. Mourloukos[1]

[1] Dpt. of Geophysics-Geothermics, National and Kapodistrian University of Athens, Greece

[2] Institute of Geodynamics, National Observatory of Athens, Greece

[3] 9 Koronidos Str., 42131 Trikala, Greece

ABSTRACT   A large amount of new and existing data was applied, aiming at delineating structural seismic risk in the earthquake prone modern city of Kalamata (SW Peloponnese) that was largely reconstructed after the devastating M_w=5.8 earthquake of September 13, 1986. Synthetic site-specific ground motion parameters derived from the nearest known shallow hazardous seismogenic sources were combined with EMS-98 structural vulnerability estimates of the city's building stock and four structural and economic loss models have been developed on a building-block scale. Assuming absence of non-linear, near-source effects, the building stock of Kalamata is anticipated to present sufficient seismic behaviour, due to the large number of new and innovative constructions replacing the demolished ones after the 1986 earthquake.

Key words: seismic vulnerability, seismic risk, economic loss, site-effects, stochastic simulation.

1. Introduction

Comprehensive seismic risk assessment, including physical and economic loss scenarios, has been performed for the modern city of Kalamata (SW Peloponnese, Greece), rebuilt after the M_w=5.8 earthquake on September 13, 1986 (Lyon-Caen *et al.*, 1988) that devastated a large part of the old city.

Seismic risk is defined as the potential structural, economic, social and environmental losses due to earthquake hazards that may occur in a specified period. The structural impact is the first constituent of seismic risk on which other losses are based. It is described as the degree of damage that assets are likely to undergo when exposed to a level of hazard. Hence, its realistic estimation is essential for stakeholders in earthquake prone urban regions in order to prioritize pre-seismic interventions and to anticipate post-seismic planning (Calvi *et al.*, 2006). However, such a task requires sufficient knowledge of a region's seismic hazard and of the elements exposed to risk, including both society and structures.

The establishment of seismic risk models in modern cities is a critical issue under constant review in developed countries. It is also of great concern for those developing countries that

suffer most from earthquakes, being vulnerable and unprepared. The effects of large disastrous earthquakes during the last decade indicate that the existing hazard models, globally, are often misleading by underestimating seismic excitations (Wyss and Rosset, 2013). Remedy to this is the current international trend for developing integrated small-scale models (Wyss and Rosset, 2013), assimilating all fundamental characteristics of a site at risk that ensure a tailor-made reinforcing of its seismic resilience.

The measured ground motions of several recent strong earthquakes in Greece were found to exceed the effective peak ground acceleration (PGA) values of the national code (e.g. Kassaras and Kazantzidou-Firtinidou, 2017); fortunately, the high quality of constructions widely prevented adverse consequences (Karantoni *et al.*, 2017). Despite this fact, until now, the seismic risk of Greece, the most seismically active region in Europe, has not been systematically investigated and targeted efforts for an intergraded assessment have been limited and inconclusive. As a result, the national seismic crisis management relies on the generic old-fashioned Xenokratis-Earthquakes Plan (2003), based on empirical constraints which at times have proven inadequate (HTC, 2014). The Xenokratis-Earthquakes Plan issued for Kalamata in 2010 is a generic adjustment of the overall Xenokratis Plan (2003) without a robust scientific background on the seismic hazard and the elements at risk (Rigopoulou, 2013).

Moreover, although the seismotectonic and geotechnical profile of Kalamata has been intensively investigated after the 1986 earthquake, a number of issues remain unanswered (EPPO, 1987). More specifically: how and to which degree the earthquake source properties, the epicentral distance, and local soil conditions, have contributed to the "irregular" damage distribution in the epicentral area, and how did the soft alluvial deposits in the coastal area contribute to the amplification of strong seismic motion.

Motivated by the abovementioned issues, we proceeded with the elaboration of the seismic risk model presented here, with the perspective that it may contribute to an innovative holistic earthquake planning and crisis management scheme for the city, when combined with proper socio-economic objectives. For the purposes of this work, we exploited a large amount of geotechnical information available for the area after the 1986 earthquake (CLPW, 1987), existing structural (EPANTYK, 2009) and damage data (EPPO, 1987) and, in addition, new geological and seismological data obtained by our working group in the framework of the GSRT KRIPIS-ASPIDA Project (ASPIDA, 2015).

Our approach includes: a) generation of deterministic site-specific ground motions using the stochastic simulation method, considering seismogenic sources by investigating the area's seismotectonics and site response functions by applying horizontal to vertical spectral ratio (HVSR) from free-field ambient noise; b) vulnerability assessment of the building stock based on the RiskUE-LM1 empirical methodology (Milutinovic and Trendafiloski, 2003) and in-situ observations; c) development of seismic risk scenarios including structural damage and economic loss for ground motion excitations generated by four scenarios of earthquakes occurring at known faults at local distances from the city. The flow chart of Fig. 1 outlines the applied methodology; in the chart, data are shown as orange boxes, methods as black boxes, results as blue boxes and future prospects as red ellipses. The derived risk outcome is released on a building block scale.

Fig. 1 - Flow chart presentation of the work.

2. Seismotectonic setting of Kalamata and the 1986 earthquake

The city of Kalamata is located ~100 km away from the SW Hellenic Arc (Fig. 2), where convergence between the Aegean-African plates occurs (Papazachos *et al.*, 2000; Laigle *et al.*, 2004; Ganas and Parsons, 2009; Kassaras *et al.*, 2016). Strong earthquakes have been reported in the area (Papazachos and Papazachou, 2003; Makropoulos *et al.*, 2012), ten of which reached a magnitude *M*≥6.0. Kalamata is surrounded by both onshore and offshore active normal faults that are classified in two categories: major west-dipping faults, oriented NNW-SSE, and south-dipping, secondary ones, oriented roughly E-W (Fig. 2). Recent geological observations (Ganas *et al.*, 2012; Fountoulis *et al.*, 2014; Valkaniotis *et al.*, 2015; Zygouri *et al.*, 2015) indicate a seismic magnitude potential M_w=5.8-6.6 for these structures. The area belongs to zone II of the Greek seismic code (EAK2000, 2003) predicting PGA=0.24 g.

Kalamata has been the subject of detailed investigation after the last devastating M_w=5.8 earthquake of September 13, 1986 (Lyon-Caen *et al.*, 1988). Damage was extensive in most parts of the town, as well as some nearby villages, and 20 people lost their lives while 330 were injured (Anagnostopoulos *et al.*, 1987). Maximum macroseismic intensity, I_0, in the Modified Mercalli Intensity scale (MMI) was assessed as I_0=IX+ (Leventakis *et al.*, 1992; Pomonis *et al.*, 2012). The greatest aftershock with M_w=5.4 occurred two days later, causing 37 more injuries and further damage to the already weakened buildings (Pomonis *et al.*, 2012). 4,495 destroyed buildings were the cumulative effect of the mainshock and its major aftershocks in the epicentral area (Argyrakis *et al.*, 1987). Given the extent of damage,
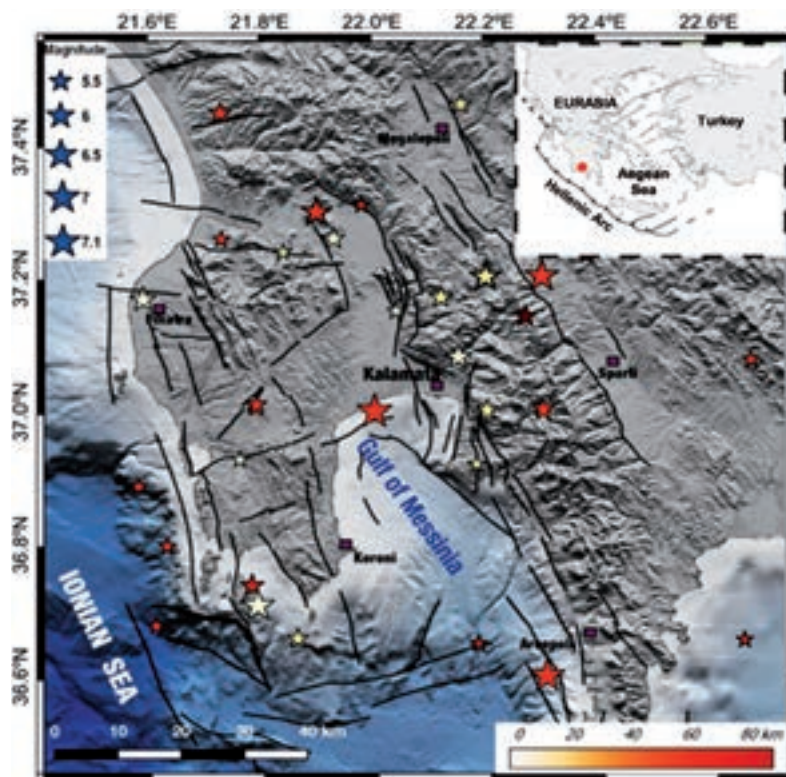
Fig. 2 - Earthquakes with *M*≥5 (stars) for the period 600 BC-1900 AD (Papazachos and Papazachou, 2003) and 1900-2009 (Makropoulos *et al.*, 2012), and active faults in the region [black lines, ASPIDA (2015)]. Star colour indicates hypocentral depth. The inset box (upper right) shows the location of Kalamata (red dot) within the Aegean plate, close to the Hellenic Arc.

casualties were relatively low due to the time of the day that the earthquake occurred (17:24:34.6 UTC) and because many collapses occurred during the aftershocks, when most of the buildings had already been evacuated. In summary, the earthquake caused major structural effects; in particular, 20% of the 9,124 buildings of Kalamata were demolished, 16% sustained serious damage, 36% suffered slight damage and only 28% remained intact (Papazachos and Papazachou, 2003).

3. Seismic hazard analysis

The comprehensive understanding of the effects of earthquake ground motion on structures is an issue that requires a multi-disciplinary approach. Effective seismic hazard analysis (SHA) in a region results from broad constraints, provided by seismology, geology, active tectonics, and local soil conditions. In the next sections, we describe the performed analysis per constituent module leading to forecasting ground motions for Kalamata.

3.1. Stochastic simulation of ground motion

Due to the sparsity of earthquake ground motion recordings in Kalamata, synthetic ones were produced using the stochastic simulation method. A detailed description of the stochastic method

can be found in Boore (1983), Beresnev and Atkinson (1997), and Motazedian and Atkinson (2005). The finite source stochastic model was applied, as it was implemented in the EXSIM algorithm (Boore, 2003, 2009), an improved version of the methodology proposed by Motazedian and Atkinson (2005). In this method, the rectangular fault plane is divided into small subfaults, where each one is considered a point source characterized by a ω^2 spectrum (Brune, 1970). The rupture starts at the hypocentre and propagates radially, triggering slip on the subfaults when it reaches their centres. One disadvantage of the procedure is that the problem of non-linearity, related to near-source effects, is not resolved by this method.

The shear wave acceleration spectrum of the ij^{th} subfault, with i and j corresponding to the subfaults coordinates on the fault plane, is derived from the point source model (Boore, 1983) expressed as (Motazedian and Atkinson, 2005):

$$A_{ij}(f) = CM_{0ij}H_{ij}\frac{(2\pi f)^2}{1+\left(f/f_{0ij(t)}\right)^2}\exp\left(-\frac{\pi f R_{ij}}{\beta Q(f)}\right)G\left(R_{ij}\right)D(f)\exp(-\pi f \kappa_0), \qquad (1)$$

where $C = \dfrac{R_{0\varphi}FV}{4\pi\rho\beta^3}$, $R_{0\varphi}$ is the radiation pattern, ρ is the density and β is the shear-wave velocity of the medium between the source and the bedrock beneath the site, F is the free surface amplification, V is the partition of energy into two horizontal components, M_{0ij}, f_{0ij} and R_{ij} are the ij^{th} subfault's seismic moment, dynamic corner frequency and distance from the observation point, respectively. The first exponential term in Eq. 1 represents attenuation of the wave with distance; $Q(f)$ is the quality factor, $G(R_{ij})$ is the geometric spreading factor, $D(f)$ is the site amplification, and $exp(-pf\kappa_0)$ is a high-cut filter to include the spectral decay at high frequencies, quantified by the κ_0 factor of soils (Anderson and Hough, 1984).

The described model is valid only when region- and site-specific controlling parameters have been suitably selected. The region-specific input parameters are: the quality factor Q, the geometric spreading factor G, the focal depth, the geometry of the fault plane, the stress parameter ($\Delta\sigma$) that defines the dynamic corner frequency f_{0ij}, and the site amplification function $D(f)$.

To estimate the expected level of ground shaking, we selected four scenarios (Table 1), inferred by the seismotectonic setting of the area (Lyon-Caen *et al.*, 1988; ASPIDA, 2015; Valkaniotis *et al.*, 2015; Zygouri *et al.*, 2015). Given the lack of rupture histories, the dimensions of uniform sources in EXSIM were set according to the magnitude potential assuming empirical relations (Wells and Coppersmith, 1994).

3.2. Ambient noise HVSR

Site amplification in the stochastic simulation was approximated by ambient noise HVSR following Nakamura's popular HVSR methodology (Nakamura, 1989, 2000). The concept is based on the phenomenon responsible for the amplification of seismic excitations over soft sediments that is the trapping of seismic waves due to the impedance between sediments and the underlying bedrock (e.g. Ansal *et al.*, 2004). Theoretical and experimental studies confirm the relevance between the fundamental frequency of ambient noise HVSR and the one of the superficial soil layers of the site (Konno and Ohmachi, 1998). The method is not generally able to provide an accurate estimate of the site amplification in cases of strong seismic excitation, as near-source effects and non-linear soil response may severely impact the seismic field (Bonnefoy-

Table 1 - Characteristics of the active normal faults for which stochastic simulation of ground motion was performed. *: Lyon-Caen *et al.* (1988), **: ASPIDA (2015). Fault strike is measured clockwise from north.

ID	Fault	Source	Strike (°)	Dip (°)	Rake (°)	Distance from Kalamata (km)	Last event	*Mw*
A (13.9.1986)	Verga	*	200	45		7	1986	5.8
B	Verga	**	200	45	-90	7	1986	6.2
C	Kourtissa	**	140	60		11	1842 ?	6.6
D	Pidima	**	200	75		8	1885 ?	6.0

Claudet *et al.*, 2006). However, given a linear response, several experimental studies revealed a satisfactory consistency between the HVSR peak values and the real site amplification (Rodriguez and Midorikawa, 2002). Ambient noise HVSR is currently one of the most popular methods for seismic site characterization in Greece (e.g. Panou *et al.*, 2005; Kassaras *et al.*, 2014, 2017).

In July 2015, a joint group of researchers from the Seismological Laboratory of the National Kapodistrian University of Athens and the Institute of Geodynamics of the National Observatory of Athens conducted a field experiment in Kalamata, collecting free-field microtremor recordings. The team carried out a series of 28 measurements at selected locations. The acquisition layout consisted of REFTEK (72A, 130) data-loggers equipped with Guralp CMG-40T and Lennartz 3D-Lite sensors. The data set was augmented by employing additional ambient noise measurements from 80 different sites within Kalamata, available from Theodoulidis *et al.* (2004).

HVSR curves were computed using the GEOPSY software suite (SESAME, 2004). GEOPSY allows the application of several processing modules (e.g. filtering, smoothing, window selection) enabling quick visualization and export of the results. The time-series were corrected for their linear trend and were tapered with a 5% cosine function at both ends. The Fast Fourier Transform (FFT) was calculated for each component and the spectra were smoothed using a Konno and Ohmachi (1998) logarithmic window. The procedure was applied to stationary noise windows of variable length, after removing transients through STA/LTA anti-triggering. The HVSR was determined by the ratio between the geometrical mean of the two horizontal components and the vertical one for each selected signal window.

Fig. 3 outlines the results of the ambient noise analysis. Peak frequencies vary between 0.3 and 5.4 Hz, whilst the greatest part of the city is founded on soils that amplify frequencies >1 Hz (Fig. 3a). Following the rule of thumb which roughly defines the eigenfrequency f_o of structures, f_o (Hz) $\sim 10/n$, where n is the number of storeys, the inferred peak frequencies may be unfavourable for constructions having more than 2 storeys. Given that the city's building stock consists of up to 5-storey constructions, low frequency peak values (<1 Hz) (Fig. 3a), possibly associated with deep formations and unlikely to be modelled by our data, are considered trivial and therefore are not further discussed. The largest amplification is observed at the coastal area (Fig. 3b), where peaks are in the range 1-2 Hz (Fig. 3a), away from the apparent elastic response (>2 Hz) of its current building stock, consisting of low-to-moderate height buildings, thus soil-structure resonance phenomena are likely not expected to occur.

Higher frequency HVSR peaks between 3 and 5.4 Hz (orange-red symbols of Fig. 3a and greenish symbols of Fig. 3b) are distributed consistently with MMI observations (Leventakis
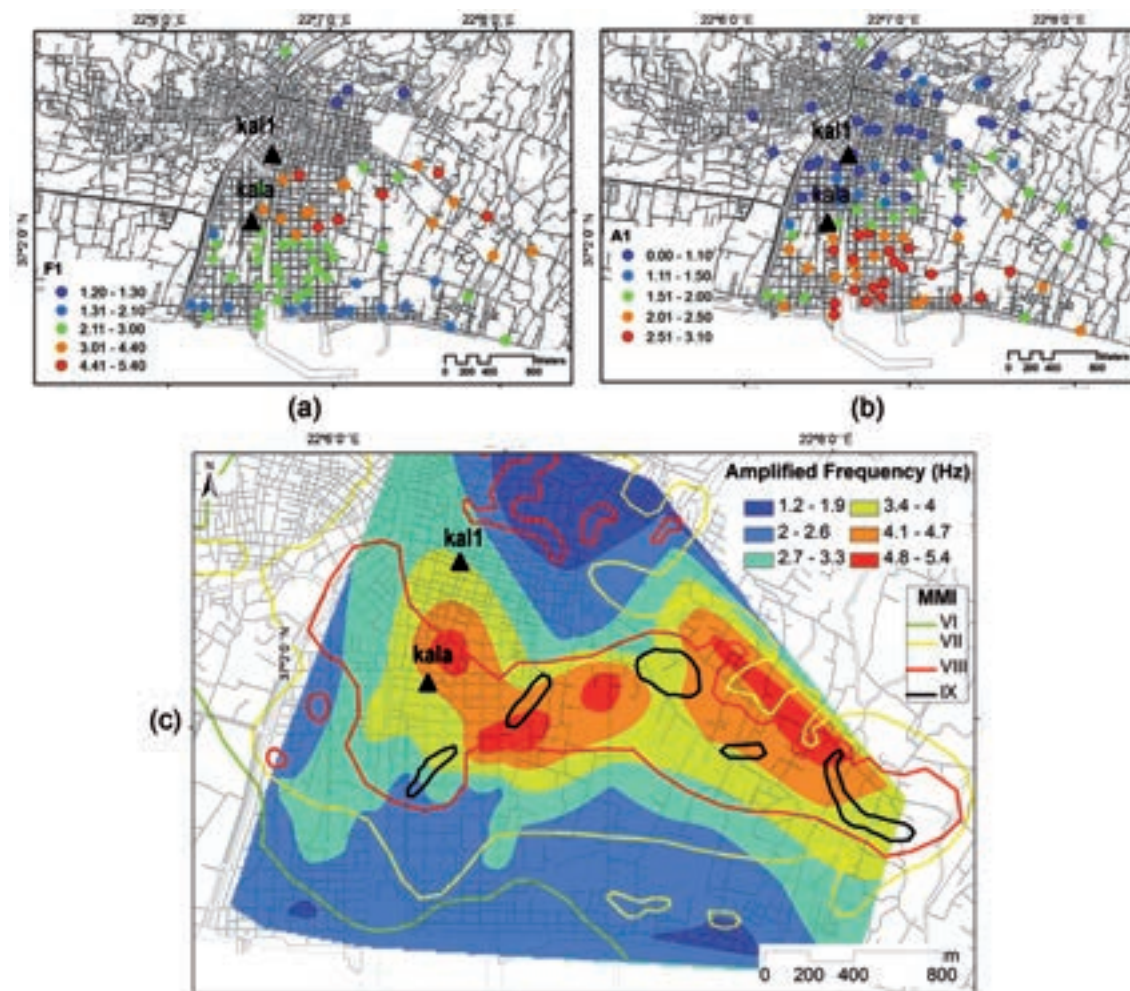
Fig. 3 - Spatial distribution of ambient noise HVSR: a) dominant frequencies at sites for which HVSR curves present discrete peaks; b) amplification ratios for all sites; c) macroseismic intensity contours (MMI) for the 1986 event (Leventakis *et al.*, 1992) overlying the distribution of amplified HVSR frequencies (coloured areas). Dots in panels a and b represent ambient noise measurements conducted by both our research group in 2015 and Theodoulidis *et al.* (2004). Black solid triangles indicate Kal1 and Kala permanent strong motion instruments of NOA and EPPO-ITSAK, respectively, that recorded the 1986 earthquake.
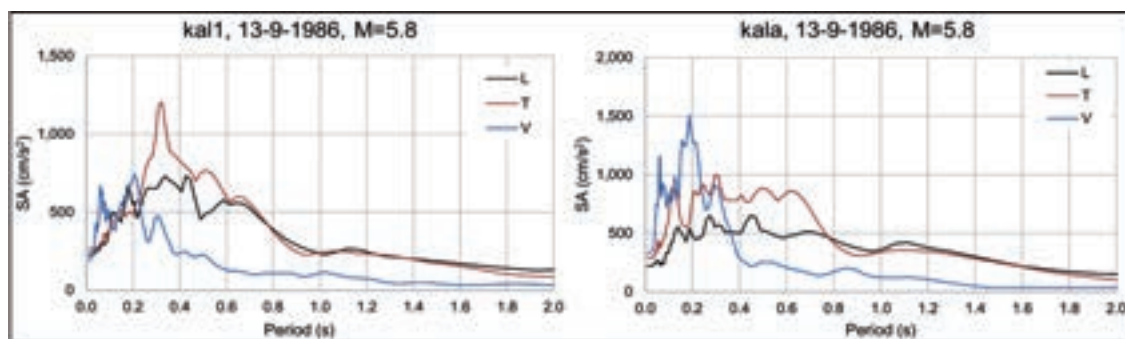

Fig. 4 - Acceleration response spectra (viscous damping ratio *h*=0.05) computed using the ViewWave algorithm (Kashima, 2007) for the recordings of the M_w=5.8 Kalamata earthquake on September 13, 1986 at Kal1 and Kala (see Fig. 3).

et al., 1992) (Fig. 3c), associated with eigenfrequencies of 2- and 3-storey buildings that were mostly affected during the 1986 earthquake. It is noteworthy that strong motion recordings of the September 13, 1986 earthquake at Kala and Kal1 accelerometric stations present peak spectral acceleration between 0.2 and 0.4 s (3-5 Hz, Fig. 4), similar to the ones derived at the central sector of Kalamata from the ambient noise analysis (Figs. 3a and 3c).

3.3. Simulation of the September 13, 1986 M_w=5.8 Kalamata earthquake (Scenario A)

The source model of the September 13, 1986 M_w=5.8 Kalamata earthquake (Lyon-Caen *et al.*, 1988) was considered for defining and validating the EXSIM empirical input parameters. The path attenuation $Q(f)$ (Eq. 1) was set after Margaris and Boore (1998). Since the short distance simulations are sensitive to the near surface attenuation, these are controlled by the parameter κ_0 (Eq. 1), a filter of high frequencies of the acceleration spectrum. Given that this parameter varies across literature, even for the same type of soil (Ktenidou *et al.*, 2015), the trial-and-error method was applied to select the most appropriate κ_0 value (Figs. 5c and 5d). The main input parameters to the EXSIM model that were found to reasonably represent the recordings of the 1986 event are given in Table 2.

Table 2 - Basic input parameters employed in the EXSIM stochastic simulation.

Parameter	Value
Stress parameter	56 Bar
Shear wave velocity	3.4 km/s
Density at source depth	2.7 gr/cm^3
Site parameter (κ_0)	0.025 s
Path properties	Q = 88 (f/1.0)$^{0.9}$ f $\geq$ 0.6 Hz
Fault plane: Strike/Dip	201°/45°
Depth of upper edge of the fault	0 km
Subfault length/width	2.5 km

Site-specific ground motions were determined in terms of Peak Ground Acceleration (PGA). The simulated motions are in agreement with the acceleration recordings of the 1986 earthquake at station Kala (Fig. 5c) and Kal1 (Fig. 5d) for both amplitude and frequency. Goodness of fit in terms of the ratio between recorded and simulated motion (Fig. 5e) presents some inconsistency in the frequency range <2 Hz, since observed ground motions appear larger than the simulated ones, especially for station Kala. This might imply that low frequency excitations, typically observed for large earthquakes (e.g. Margaris and Hatzidimitriou, 2002), are likely related to near field seismic motions. For frequencies >2 Hz, the synthetic PGA values are comparable with the real recordings.

3.4. Simulation of three future earthquake scenarios

Ground motions for three hypothetical future earthquakes occurring on fault sources close to Kalamata (Fig. 5a) were generated using EXSIM. The average magnitude for each fault source was considered after ASPIDA (2015) (Table 1). Thereafter, synthetic ground motions were determined at 108 locations in Kalamata by employing the HVSR curves as site amplification functions. Absolute PGAs of the synthetic accelerograms were, then, combined in a GIS scheme using the natural neighbour approach (Sibson, 1981). Fig. 6A presents the results of the simulation showing that the absolute PGA values regarding the scenario of the 1986 earthquake range between 120 and 600 cm/s^2.
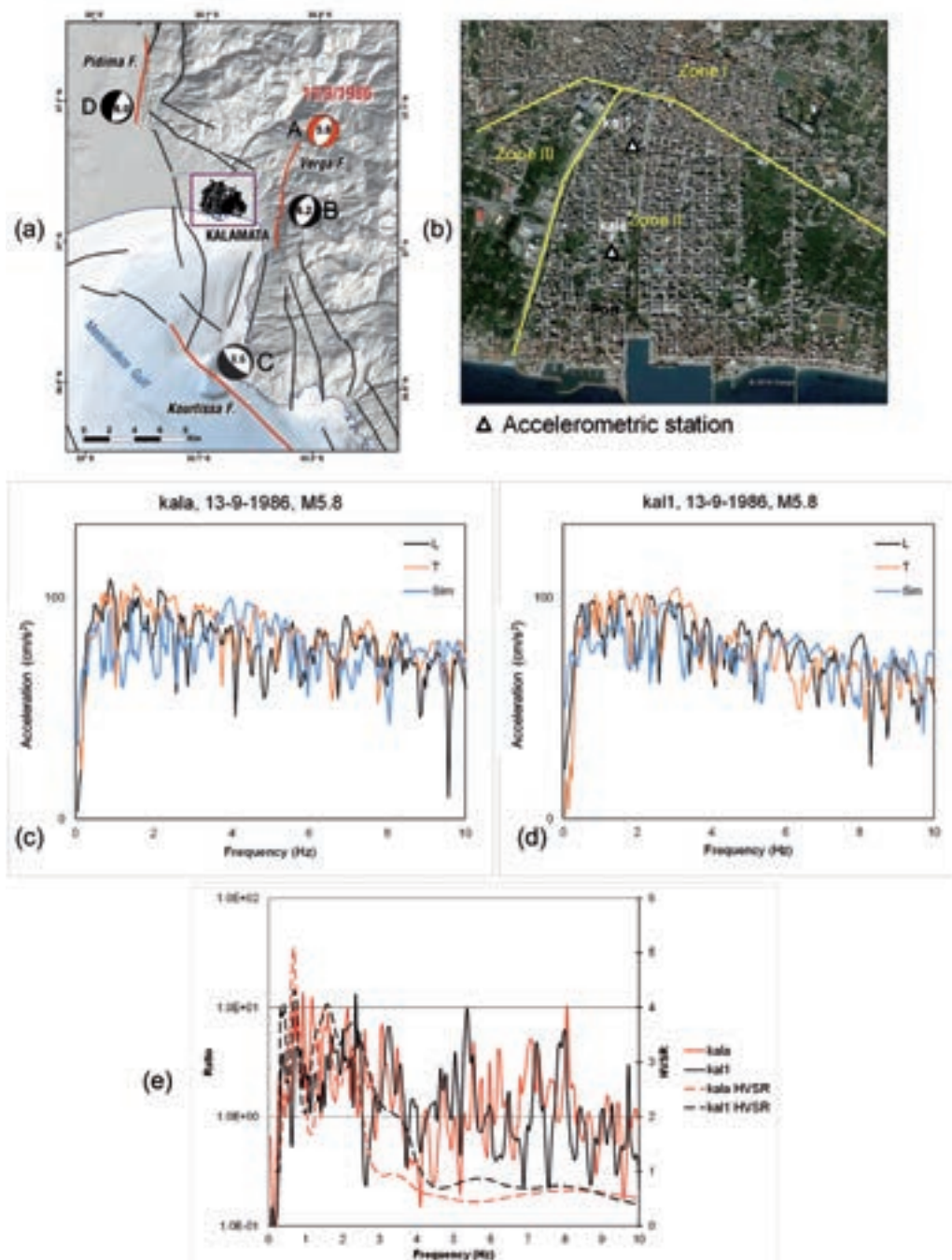
Fig. 5 - a) Map showing onshore and offshore active faults near Kalamata [black lines, ASPIDA (2015)]. Beach-balls indicate the focal mechanism of each earthquake for which strong ground motion was simulated (red lines). Numbers in the middle of the focal spheres indicate the earthquake magnitude of each scenario. Letters (A-D) indicate the scenario ID (Table 1). b) Location of the accelerometric stations Kala and Kal1. Yellow lines indicate zones (I-III) in which the area was divided on the basis of the characteristic oscillation period of the soil column (Boukovalas and Sabatakakis, 1987). c, d) Fourier spectra for the September 13, 1986 earthquake recordings and the simulated motion, respectively. Acceleration axis is in logarithmic scale. e) Ratio (left axis) of the average recorded horizontal acceleration to the respective simulated acceleration of the 1986 earthquake (solid lines). Dashed lines are HVSR (right axis) of the earthquake recording.

For the city of Kalamata, PGA is found in the range 240-360 cm/s^2, in agreement with the instrumental observations. Maximum peak values are observed in the vicinity of the causative Verga fault.

Scenario B: M_w=6.2 future earthquake on Verga fault (Fig. 6B). This is the worst-case scenario for the target site. The retrieved values of the absolute PGA in the broader area range between 240 and 920 cm/s^2, greatly exceeding the maximum values of the effective PGA of the seismic code (EAK2000, 2003). Maximum values are presented towards the east, near Verga fault. The city of Kalamata is subjected to PGA in the range of 240-600 cm/s^2. Relatively high values (360-480 cm/s^2) are observed at the southern part, reflecting poor soil properties, in agreement with EPPO (1987).

Scenario C: M_w=6.6 future earthquake on Kourtissa fault (Fig. 6C). The values of the simulated absolute PGA in the broader area range between 120 and 480 cm/s^2. The respective PGA in the city of Kalamata is in the range of 240-360 cm/s^2, exceeding the maximum effective values indicated by the current seismic regulation (240 cm/s^2) (EAK2000, 2003). The maximum values are found in the southern and eastern part of the city and further eastwards. Smaller values are mainly in the north and west of the city.

Scenario D: M_w=6.0 future earthquake on Pidima fault (Fig. 6D). This is the most amenable scenario for the city of Kalamata. The values of the simulated absolute PGA range between 120 and 240 cm/s^2, being below the effective PGA values of EAK2000 (2003).
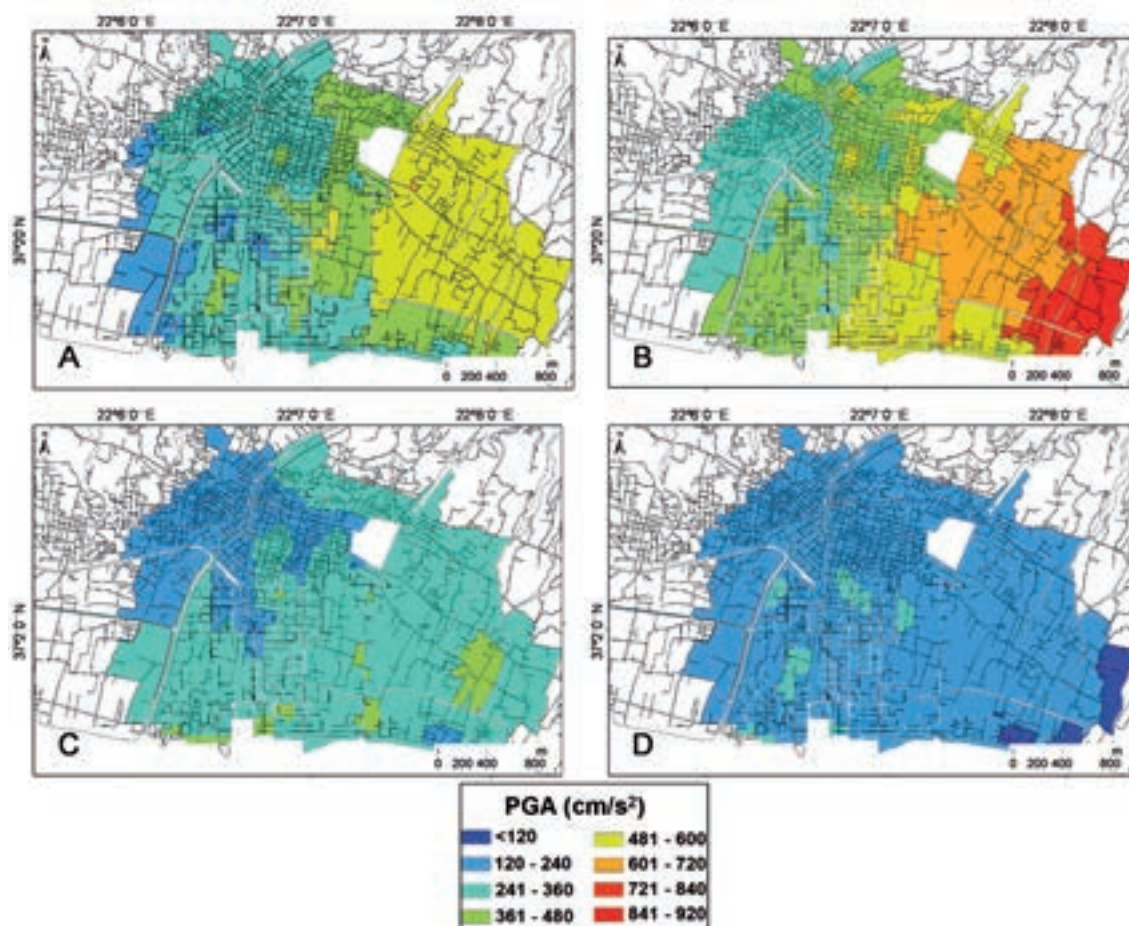

Fig. 6 - Scenario shakemaps in Kalamata. The parameters for each scenario are presented in Table 1.

4. Geotechnical modelling of Kalamata

In this section we describe the analysis on assessing the dynamic characteristics of the subsoil of Kalamata. To this end, we exploited the numerous microtremor measurements, new geological observations (ASPIDA, 2015) and existing geotechnical/geophysical data available from the multidisciplinary research conducted after the 1986 earthquake. The latter were employed to constrain a representative model for the region, serving as a realistic starting model in the random perturbation (Monte-Carlo) procedure described below.

The analysis of soil profiles CLPW (1987) and field mapping in the framework of ASPIDA (2015) imply that the stratigraphy of Kalamata is complex, related to a mild topography and the deposition process by the Nedon River alluvial fan (Fig. 7). More specifically, the soil formations in Kalamata are subdivided into five units:

I - *Sand, sand mud and sand gravel unit*. This is exposed at the west and the south part of the city having a maximum thickness of 20 m; elsewhere the thickness varies between 3 and 5 m. This formation is related to EAK2000 (2003) - Γ and X soil classes.

II - *Low plasticity clay with sand unit*. This appears at the western part of the old city [EAK2000 (2003) - B and Γ soil classes, Fig. 7], having a maximum thickness of 18 m. It is an inhomogeneous, dense and stiff formation.

III - *Mixed phase comprising sand, rubble and mud aggregates*. This presents low-to-medium plasticity and its thickness varies 3-40 m [EAK2000 (2003) - Γ soil class].

IV - *Moderate-to-well adhered, mixed conglomerate*. This is taken as a refusal on Standard Penetration Tests (SPT). The thickness of the formation ranges between 2 and 10 m [EAK2000 (2003) - A and B soil classes].

V - *Marls*. A rather high number of SPT (N_{SPT}) values were found for this formation. Its thickness is not assessed by the geotechnical drilling. Marls are exposed at the northern part of the city [EAK2000 (2003) - A1 and A2 soil classes], slightly deepening towards the coast. Depth in some areas extends to more than 70 m.

Fig. 7 presents the simplified geotechnical map of Kalamata based on field mapping in the frame of the current work, showing that the city lies on medium hard (B) soft (Γ) and poor (X) soils. Soil classification is based on EAK2000 (2003) classification scheme, as follows: A1 - Hard bedrock exposures, A2 - Sediment formations with thickness of 0 - 21.5 m, B - Sediment formations with thickness of 21.5 - 40 m, Γ - Sediment formations with thickness of more than 40 m and X - Loose sands susceptible to liquefaction (coastal deposits and river beds). In the figure, locations of stations Kala and Kal1 are indicated. According to our survey, this shows that they lie marginally on different soil categories B and Γ, respectively, which possibly explains the different characteristics of the two recordings.

4.1. Inversion of ambient noise HVSR curves

We applied Herak's ModelHVSR code (Herak, 2008). The algorithm is based on the assumption that the peak of the HVSR is caused by incident body waves, specifically by multiple reflections of *S*-waves (Nakamura, 2008). It involves a Monte-Carlo (random) perturbation between an observed HVSR curve and a user-defined 1D viscoelastic model that consists of horizontal isotropic soil layers overlying elastic half space, searching for the best-fit soil column. Each horizontal layer in the scheme is defined by its thickness, P- and S-wave velocity, density and the
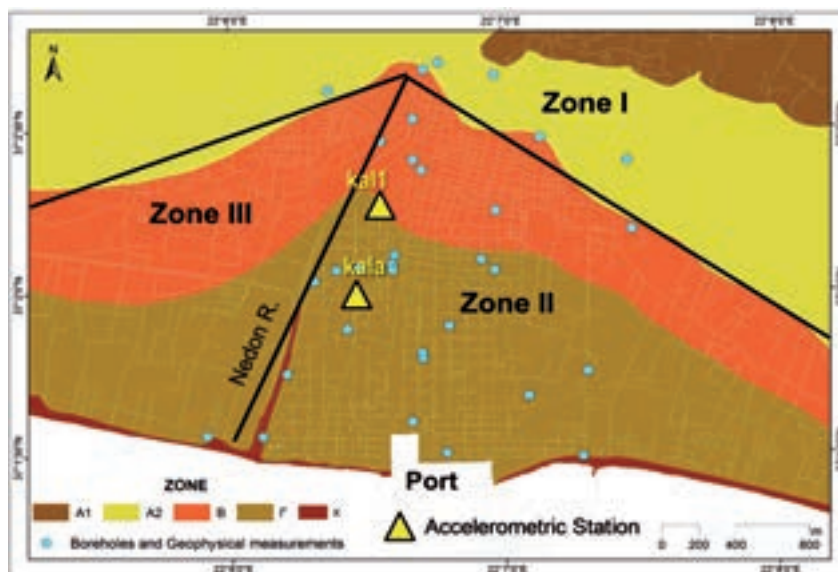
Fig. 7 - Geotechnical setting and microzonation of Kalamata (approximate zones I-III, EPPO, 1987). Colour classes (A1, A2, B, Γ and X) are the soil classification after EAK2000 (2003) based on field mapping in the frame of the current work.

frequency dependent *Q*-factor which controls the inelastic properties of the wave propagation in each layer. Average *Vs* for each of the five geological layers of the soil was estimated (Table 3) by applying empirical formulas (Kalteziotis *et al.*, 1992; Lotzetidis *et al.*, 1992; Tsiambaos and Sabatakakis, 2011) which relate *Vs* to N_{SPT} values, averaged over 33 boreholes available from CLPW (1987).

It is worth noting that the indirect association between *Vs* and N_{SPT} as well as their averaging, involves significant biases originating from the heterogeneity of boreholes related to the complexity of the sub-surface of Kalamata (CLPW, 1987). Therefore, the 1D generic soil column acquired from borehole data (Table 3) is only indicative, adopted mainly for calibrating the viscoelastic parameters of the best-fit models derived from the inversion of the ambient noise HVSR curves. Given these limitations, extensive analysis for correlating geotechnical and ambient noise HVSR soil dynamic response is required, which is beyond the scope of this work, being considered, however, as a future research task.

In the procedure, only 34 HVSR curves having clear peaks at a ratio ≥2 were considered for the site characterization according to the guidelines of SESAME (2004). The HVSR curves were classified into distinct groups, based on spectral shape similarity. Correlation coefficient measurements were performed on the smoothed HVSR spectra, over their log-amplitudes after subtraction of their mean values, and clusters were formed by applying furthest neighbour linkage with a fixed threshold value of 0.8. The method yielded 28 groups of HVSR curves, 8 of which involve spectra with sharp peaks at a ratio ≥2. Their spatial distribution is shown in Fig. 8. Only these HVSR curves were used in ModelHVSR together with the starting mean geotechnical model, which was randomly perturbed towards determining site-specific best-fit 1D models of the soil column. 74 HVSR curves presenting low ratios (<2) and/or no clear peaks were excluded from the analysis.

At a first stage, an average HVSR curve was constrained for each subgroup of the selected

curves that was input in the ModelHVSR procedure; 5000 random perturbations per dataset yielded 8 viscoelastic models (Table 3). The values of the elastic parameters of the derived 1D models (Vs, thickness, density ρ) lie in a realistic range and they are comparable with the average 1D model deduced from borehole data (Table 3).

However, the procedure of inverting a multilayer 1D soil column on the basis of ambient noise HVSR curves, simplified by a Konno and Ohmachi (1998) smoothing, is not straightforward. This is because the obtained curves represent only the response of the whole soil column, hence the response of the upper soil layers related to higher oscillation modes cannot be retrieved. Therefore, each 1D model in Table 3 has been averaged in a typical Vs_{30} approximation, i.e. the average shear-wave velocity between 0 and 30 m depth.

The outcome of the analysis presented in Table 3 implies soil quality EC8 (CEN, 2002) C and D for the southernmost part of Kalamata. Vs_{30} of the 8 average 1D models is found in the range 155-210 m/s. Amplification of the *SH* incident waves due to a regolith overlying hard bedrock of category A (A_{soil}/A_{rock}) is calculated by ModelHVSR 2.7-3.3, at epicentral distance 7 km from a *M*=6.0 earthquake with a hypocentral depth of 10 km (Fig. 9). These values are higher than the generic ones determined by Pitilakis *et al.* (2012) for EC8 C and D soil categories using acceleration records from a global strong-motion database. Nevertheless, besides the uncertainties of the applied methods, it is considered that the outcome adequately represents the dynamic properties of the soil columns at the investigated locations.

The next step was to invert each *k-th* HVSR curve using the 1D average soil column of the *k-th* HVSR cluster as an initial model (as listed in Table 3). The procedure yielded 34 1D 5-layer viscoelastic models, simplified into Vs_{30} models due to the reasons explained above. Fig. 10a shows the distribution of the derived Vs_{30} values at 34 locations and Fig. 10b presents the corresponding EC8 soil classification. Vs_{30} ranges between 140 and 230 m/s corresponding to soil categories C and D. The lowest Vs_{30} values are found near the coastal area. At several sites, Vs_{30} values are found close to 180 m/s, marginal to categories C (180 m/s< Vs_{30}≤360 m/s) and D (Vs_{30}≤180 m/s). The obtained configuration is in agreement with the EAK soil category Γ found at the southern part of Kalamata. Further north, we interpret the lack of soil characterizations, i.e. excluded HVSR curves with low values, due to stiff formations compatible with EAK2000 (2003) A and B soil categories (Fig. 7).
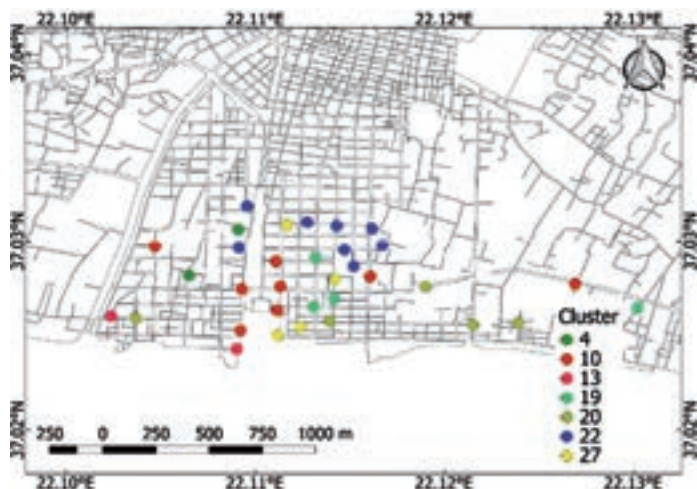

Fig. 8 - Distribution of the selected 34 HVSR curves used in the ModelHVSR analysis and their classification in clusters according to their spectral shape similarity.

Table 3 - *Vs* soil column models in Kalamata deduced from geotechnical borehole SPT data and viscoelastic parameters derived by the inversion of 8 average HVSR curves using the ModelHVSR algorithm (Herak, 2008).

Dataset	Thickness (m)	*Vs* (m/s)	ρ (gr/cm³)	Q_p	Q_s	V_{S30} (m/s)	EC8 class	Amplification (A_{soil}/A_{rock})
Boreholes	12.0	266	1.90	30	10	280	C	1.35
	8.6	333	2.10	30	10			
	13.0	348	2.20	30	10			
	15.0	414	2.30	30	10			
C004	4.0	159	1.84	25	10	205	C	2.80
	12.8	167	2.07	63	18			
	25.6	391	2.13	64	20			
	40.6	561	2.08	90	38			
	∞	1500	2.40	100	50			
C010	5.6	175	1.77	25	10	210	C	2.90
	16.4	187	1.99	50	11			
	31.4	344	2.00	50	11			
	46.4	1049	2.00	81	27			
	∞	1500	2.40	100	50			
C013	5.6	171	1.60	26	10	200	C	3.40
	16.4	174	1.61	47	10			
	31.4	339	1.95	93	19			
	46.4	563	2.00	93	24			
	∞	1500	2.40	100	50			
C019	6.7	137	1.76	24	10	180	D	2.70
	15.3	163	1.99	47	12			
	30.3	350	2.00	61	12			
	45.3	541	1.99	61	40			
	∞	1500	2.40	100	50			
C020	10.8	122	1.82	43	10	155	D	2.80
	19.4	180	2.18	43	10			
	32.4	543	2.18	43	13			
	47.4	580	2.19	46	11			
	∞	1500	2.40	100	50			
C022	2.0	94	1.84	32	10	192	C	2.80
	10.6	127	2.18	52	10			
	23.6	339	2.18	54	22			
	38.6	451	2.19	62	42			
	∞	1500	2.40	100	50			
C027	5.4	120	1.78	25	10	175	D	3.30
	14.0	138	2.06	55	12			
	29.0	420	2.22	86	25			
	44.0	606	2.04	94	25			
	∞	1500	2.40	100	50			

5. Seismic vulnerability assessment

The seismic vulnerability was assessed using the RISK-UE LM1 macroseismic methodology (Milutinovic and Trendafiloski, 2003), an empirical Damage Probability Matrix (DPM) approach based on the EMS-98 macroseismic scale (Grünthal, 1998). According to RISK-UE LM1, buildings characterized by a similar seismic behaviour are grouped together into certain vulnerability classes,
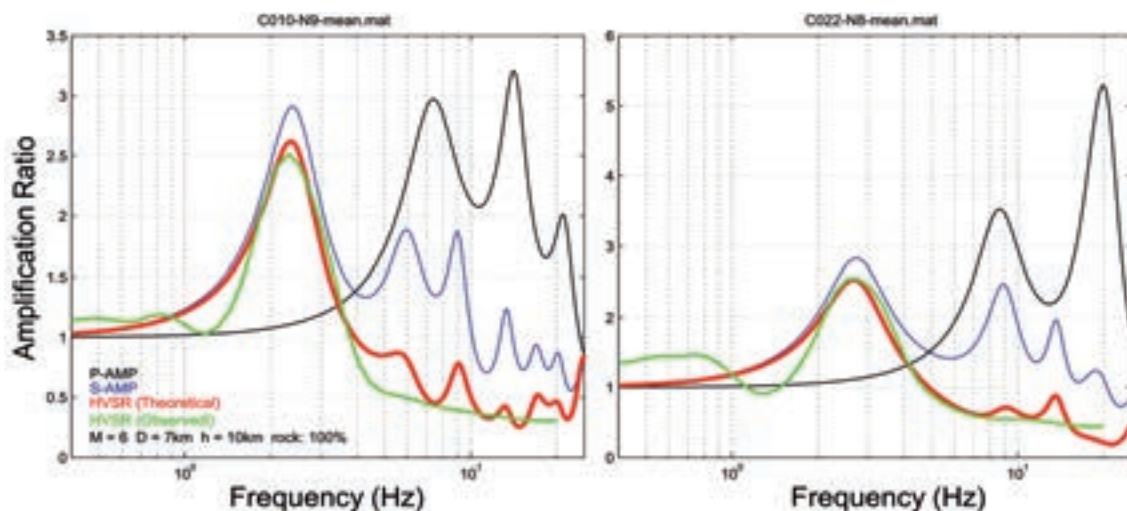
Fig. 9 - Examples of the theoretical soil response after the inversion of the average HVSR curves for clusters #10 (left) and #22 (right). Amplification ratios have been computed for a *M*=6.0 earthquake of 10 km depth at an epicentral distance 7 km. Green line is the observed averaged HSVR curve per cluster.
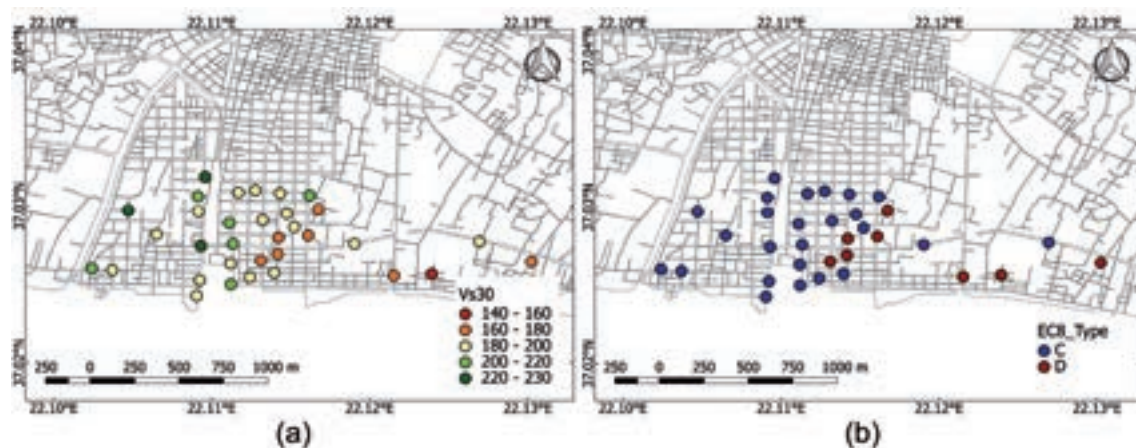

Fig. 10 - a) Distribution of Vs_{30} (m/s) and b) the respective EC-8 soil classification.

following a probabilistic approach. Thereafter, vulnerability indices, within probability ranges, are introduced to quantify the building stock classification. Modification scores are then applied, accounting for structural specificities (Giovinazzi and Lagomarsino, 2004). The RISK-UE LM1 method defines semi-empirical vulnerability functions that correlate the seismic intensity, *I*, and the vulnerability index (VI), with the mean damage grade, μ_D; μ_D ranges from 0 (no damage) to 5 (very heavy damage-collapse), *I* ranges 0-12 and VI ranges 0-1 (less-to-most vulnerable structures).

The deliverables of the research project EPANTYK (2009) were employed for constraining the city's exposure model. EPANTYK (2009) is based on structural data obtained during the 2001 census, which includes buildings characteristics, i.e. height, use, material, construction period (Fig. 11). Within the ASPIDA project, on-site validation of the provided information was performed, as well as empirical estimation of the material and the typology of the structural system. The database characterizes 7960 standard buildings, for which the main bearing system is masonry walls (stone, rarely clay/cement bricks) and reinforced concrete (RC) infilled frames. The vast majority are
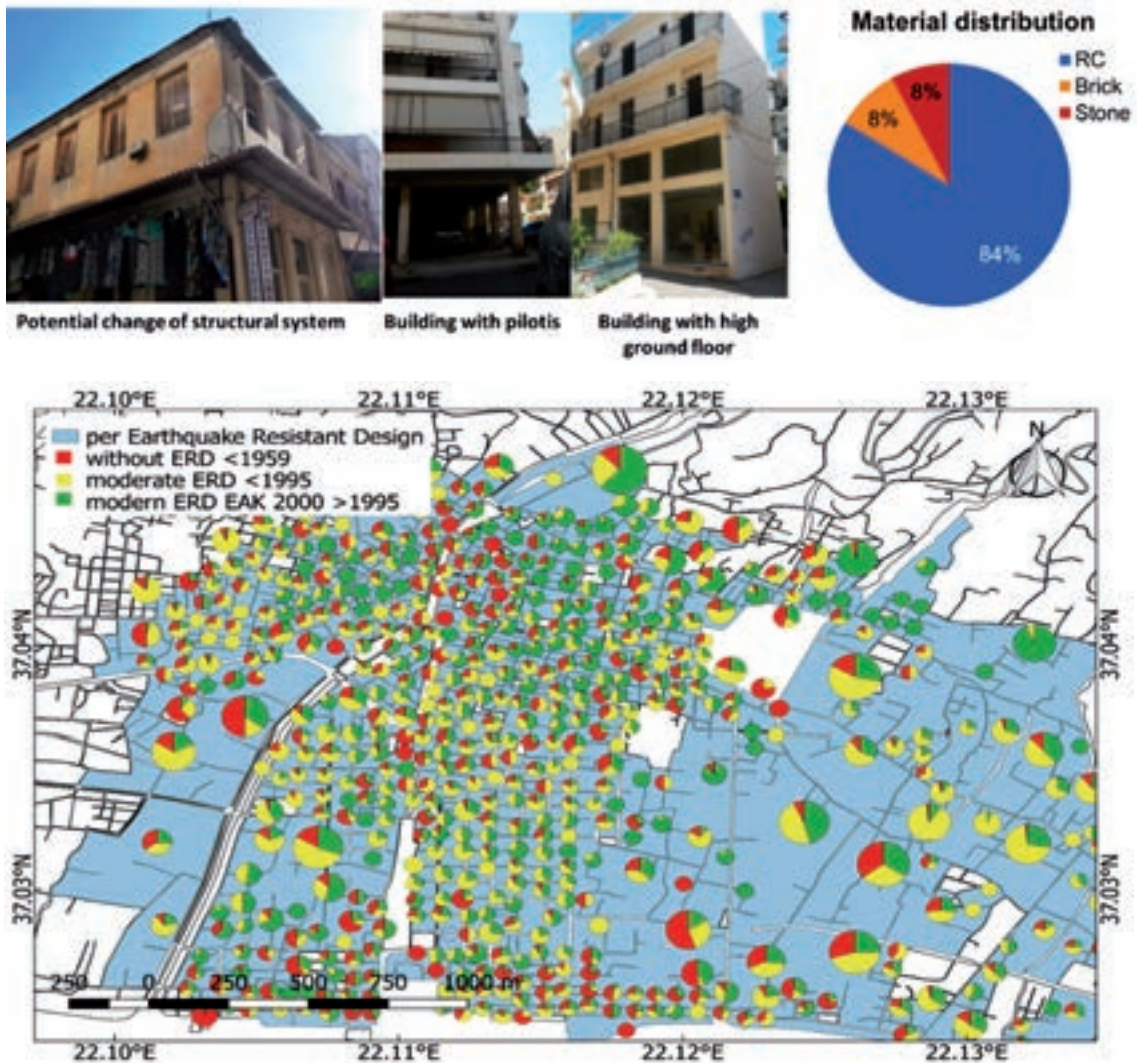
Fig. 11 - Exposure of the building stock of Kalamata. Top: field photographs of buildings and pie-chart of building material distribution (data origin EPANTYK, 2009). Bottom: map of Kalamata building blocks with/without Earthquake Resistant Design (ERD).

low-rise RC buildings of residential and commercial use. Much of the building stock was erected during the great urbanization period, between 1960 and 1970, under premature seismic provisions.

During the 1986 disastrous earthquake, ~70% of its buildings suffered moderate to very heavy damage and had been demolished/reconstructed or retrofitted. As a result, about 40% of Kalamata's building stock was strengthened, following the seismic code issued in 1985, and, consequently, the structural vulnerability of the city is currently significantly reduced.

Typological vulnerability indices were assigned to each building based on the designation of EPANTYK (2009), relative to the material and the estimated design/construction period of the constituent structures. Moreover, according to Giovinazzi and Lagomarsino (2004), structural characteristics contributing to the increase of vulnerability, such as their height, vertical irregularity, insufficient seismic joints between adjacent buildings, were applied on the vulnerability attributes by means of modification scores. Fig. 12 presents the average distribution of the structural
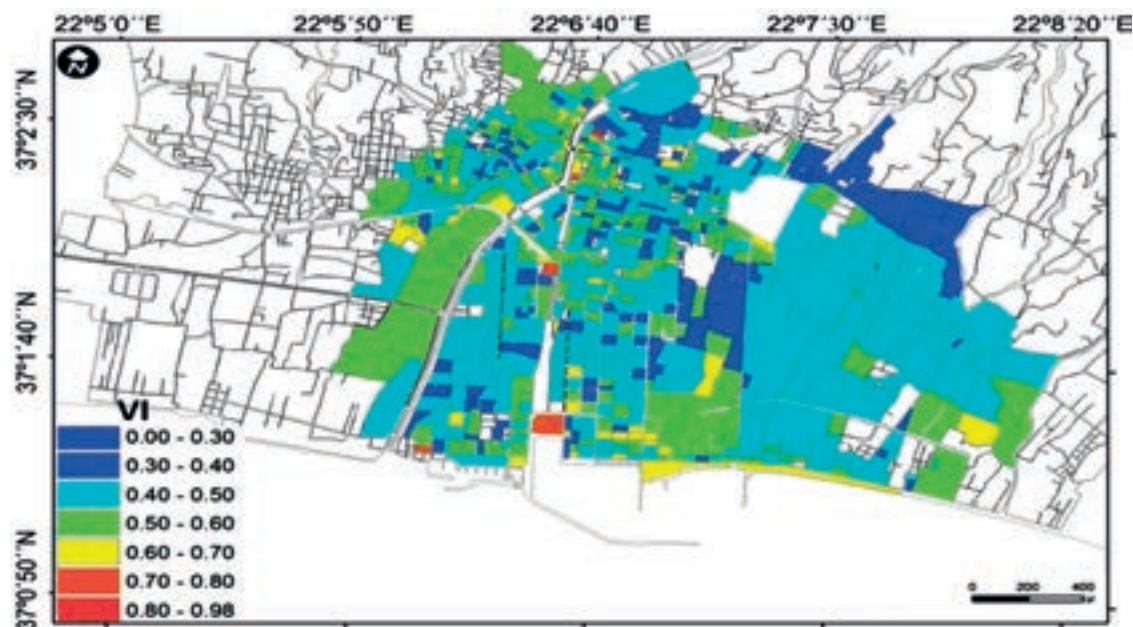
Fig. 12 - Distribution of the mean structural vulnerability index (VI) per building block in Kalamata. Blank polygons denote "No data".

vulnerability index values across the target site per building block. The majority of the building blocks has a low vulnerability index (<0.5), as the result of the city's reconstruction after 1986.

6. Seismic risk analysis

Seismic risk scenarios were developed in terms of discrete damage probability by applying the beta distribution of the mean damage grade for all damage grades. The expected mean damage grade is the result of a vulnerability function that correlates the quantified vulnerability with the macroseismic intensity (Giovinazzi and Lagomarsino, 2004). Although the analysis was performed building-by-building, seismic risk estimates are presented per building block aggregates due to restrictions on risk dissemination policy.

Specifically, the damage scenarios were elaborated by: a) attribution of the interpolated synthetic intensity to each sampled building block, b) computation of the mean damage grade per building according to the seismic intensity and the structural vulnerability, c) estimation of the probabilities of occurrence of each damage grade at building level, d) definition of the most probable damage grade per individual building or building block. Synthetic Seismic Intensity (SI) was derived by applying the empirical formula of Tselentis and Danciu (2008), found to provide realistic results for Greek regions (ASPIDA, 2015; Kassaras *et al.*, 2015).

Fig. 13 illustrates the resulted damage distributions for all buildings at block level. Scenario D leads to more favourable consequences, whereas the extreme scenario (B) depicts the highest expected damage. For all cases, the influence of the proximity to the faults is underlined, whereas near-source non-linear effects were not considered. Given the aforementioned, the expected seismic risk of the city is found to be relatively low. As presented in Table 4, scenario A (simulation of the 1986 earthquake) involves a much lower damage with respect to the one caused by the 1986 earthquake (EPPO, 1987) given the reduced inherent vulnerability of the city.
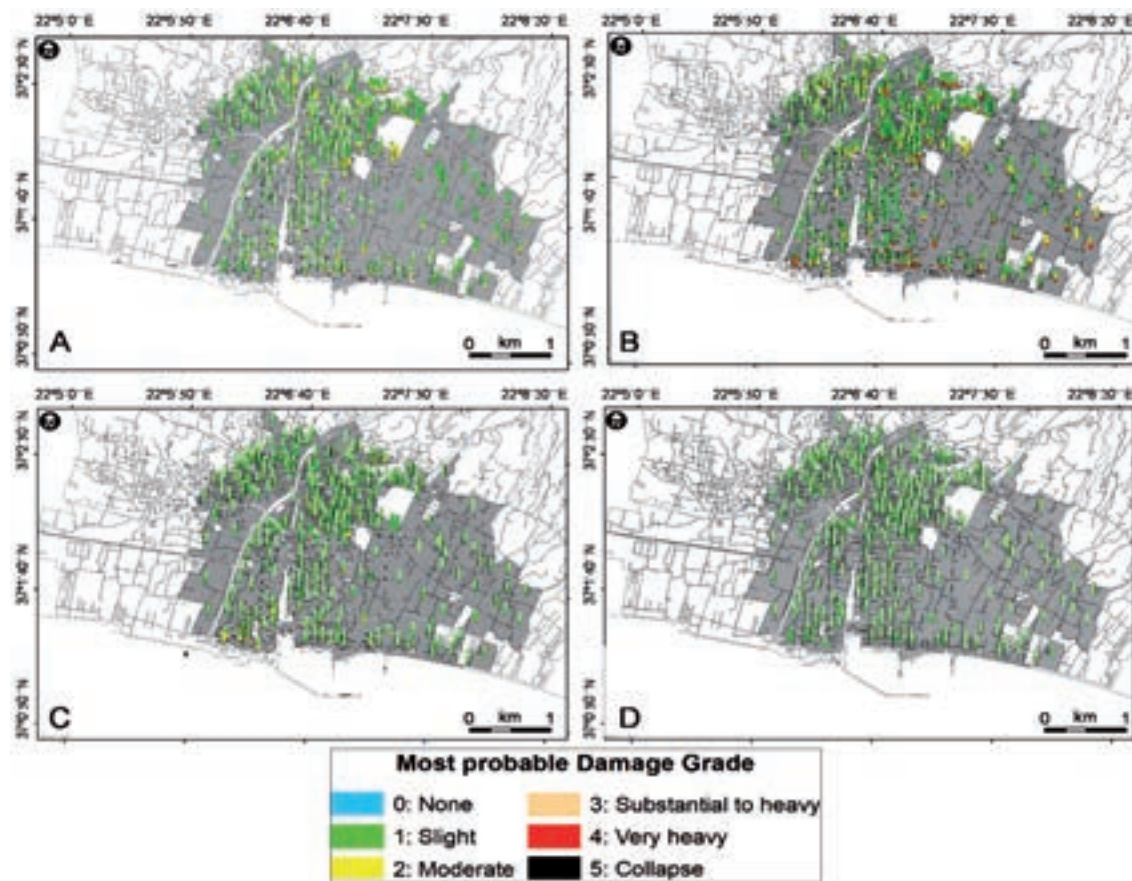
Fig. 13 - Damage distribution per building block for scenarios A-D (Table 1). Blank polygons within the urban area denote "No data".

Table 4 - Estimated ratio of damaged buildings per damage grade (DG) for the four scenarios (A-D, Table 1) and registered impact during the 1986 earthquake (EPPO, 1987)

Case	Fault/*Mw*	DG (% of total buildings)					
		0	**1**	**2**	**3**	**4**	**5**
09/13/1986	Verga/5.8	28		36	16	20	
		DG (% of total buildings)					
A	Verga/5.8	56	32	12	0	0	0
B (MCE)	Verga/6.2	29	47	18	6	0	0
C	Kourtissa/6.6	76	19	5	0	0	0
D	Pidima/6.0	85	15	0	0	0	0

7. Economic loss

The estimation of economic loss is an impact indicator providing quantitative and comprehensive information to stakeholders. According to the Earthquake Consequences Database of GEM (GEM-ECD, 1986), the direct economic loss of the earthquake of 1986, as estimated by Munich Re, was in the order of 670 million Euros.

The expected economic loss due to the implemented earthquake scenarios was estimated by combining the probabilities of occurrence of the different damage grades and the respective

damage ratio (Damage Function - DF). The latter represents a rough estimate of a building's lost surface per damage grade and has been defined by considering data from the literature, i.e. for RC structures DFs for the Greek territory have been used from Kappos and Dimitrakopoulos (2008), whereas for masonry structures, given the absence of relevant studies in Greece, the DFs of Dolce *et al.* (2006) have been adopted. Table 5 presents the ratio values deduced for each damage grade for the two main structural typologies assuming a cost replacement unit CC=A×750 €/m², where A is the building's area (in m²) susceptible to loss.

Only structural damage and direct economic loss have been taken into account. All kinds of non-structural damage due to dynamic effects have been omitted. Likewise, indirect economic loss, incorporating effects on the commercial trading, potentially vulnerable to the interruption of its operation, has not been included, as being the objective of a future study towards a holistic seismic risk plan for Kalamata.

The building block area susceptible to loss (A) was estimated by the product of each block's built surface (EPANTYK, 2009) and the average number of storeys of the buildings in the block. The probability of occurrence per damage grade for the mean damage grade μ_D per block area was then applied. The mean damage cost (or loss) ratio (%) is defined by:

$$E(C|IM) = \sum_{i=1}^{5} DF_i \times P[d_{si}|IM = I] \qquad (2)$$

The loss ratio (C) is expressed by means of vulnerability curves for all MMI intensities (IM), representative of the different building typologies. The total structural damage cost (or repair cost) CS excluding contents, is calculated by combining the total damage cost ratio with the replacement cost of a new construction (CC):

$$CS = E(C|IM) \times CC \qquad (3)$$

The expected direct economic loss of the city of Kalamata is presented in Fig. 14 and is summarized in Table 6. Although minor structural damage is most probably expected for the scenarios C (Pidima) and D (Kourtissa) (Fig. 13), the non-negligible probabilities of occurrence of higher damage should be taken into account.

Table 5 - Damage functions per damage grade for RC and masonry buildings.

Typology	DG1 (%)	DG2 (%)	DG3 (%)	DG4 (%)	DG5 (%)
Reinforced Concrete (Kappos and Dimitrakopoulos, 2008)	0.5	5.0	20.0	45	80
Masonry (Dolce *et al.*, 2006)	3.5	14.5	30.5	80	95

Table 6 - Expected economic loss per seismic scenario for the current vulnerability state of buildings.

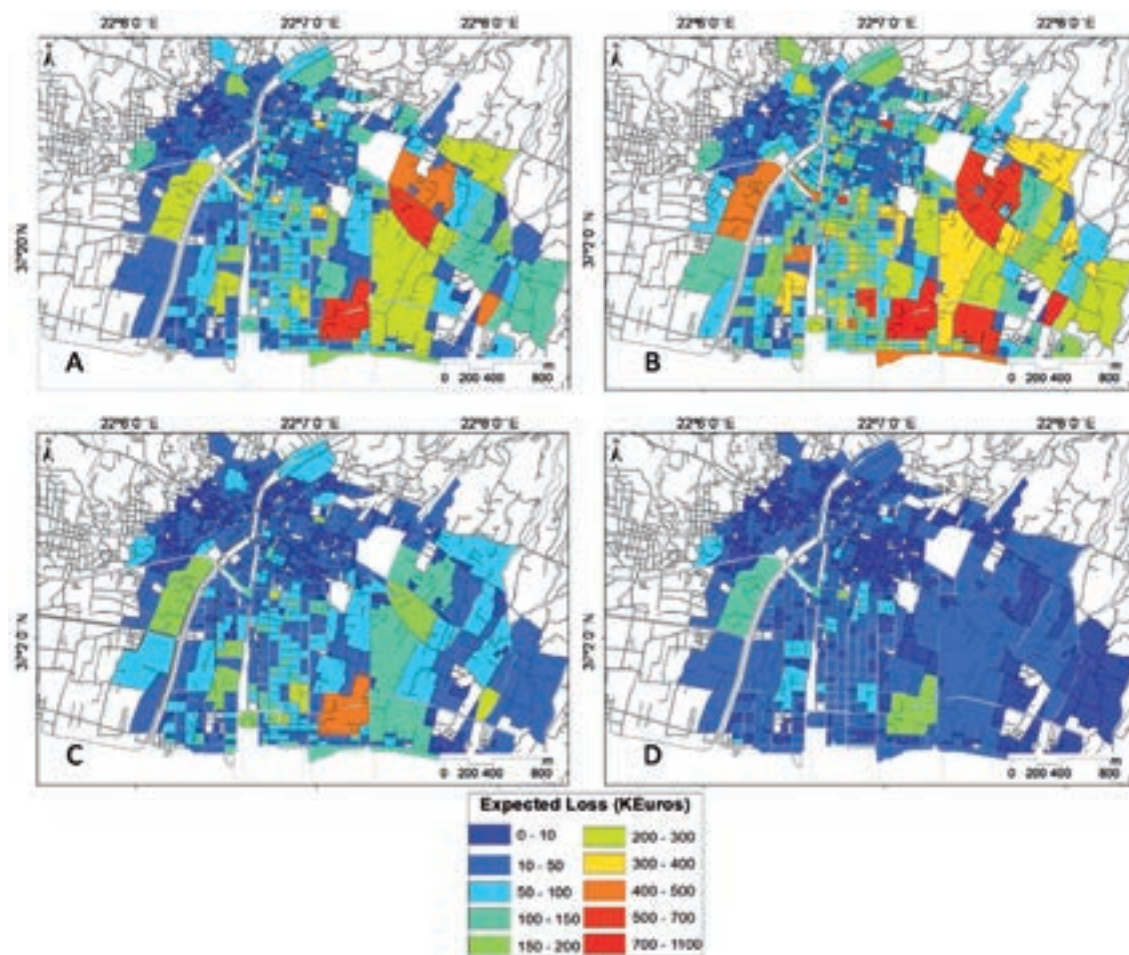| Scenario	Fault	*Mw*	Total economic loss (MEuros)
A (09/13/1986)	Verga	5.8	33
B (MCE)	Verga	6.2	60
C	Kourtissa	6.6	22
D	Pidima	6.0	10

Fig. 14 - Expected economic loss per building block for scenarios A-D. Blank polygons within the urban area denote "No data".

8. Summary and discussion

This work presents a comprehensive structural seismic risk model for the city of Kalamata, implemented by applying the following tasks:
– calculation of HVSR from ambient noise measurements;
– estimation of the geotechnical profile of the subsoil by the inversion of HVSR curves;
– validation of the parameters of the stochastic simulation model using instrumental recordings;
– stochastic simulation of site-specific ground motions for 4 scenarios of major local earthquakes;
– assessment of seismic vulnerability of the building stock;
– development of four structural seismic risk and economic loss scenarios.

The analysis of the massive data set and the applied methodology highlight several issues, the most important of which are discussed below.

Synthetic seismic motions were frequently found to exceed the provisions of the seismic code of effective PGA=240 cm/s^2, reaching values of PGA>900 cm/s^2 in the extreme scenario, with an estimated 675 cm/s^2 of effective PGA. We note that effective PGA in EAK2000 (2003), represents in general ~75% of the probabilistic PGA estimates, although there is no published explanation on the matter (Roumelioti *et al.*, 2017). The stochastically obtained values are also higher than the ones proposed by others using both probabilistic approaches (e.g. Papazachos *et al.*, 1993; Kouskouna and Kaviris, 2014; Slejko *et al.*, 2014). The above highlight the debate on the efficiency of probabilistic and deterministic approaches (e.g. McGuire, 2001), since common probabilistic methods refer to extended seismic zones, while deterministic methods are source-specific. Moreover, seismic motions are computed only for hard rock conditions, whereas excitations derived herein also include soil amplification effects.

On the other hand, the synthetics of the 1986 mainshock obtained herein are consistent with Theofanopoulos and Dan (1988), who applied recordings of aftershocks of the 1986 event as empirical Green's functions towards addressing propagation and site effects and considering a causative fault of a total surface ~100 km^2. On the contrary, Kouskouna and Kaviris (2014) by applying a deterministic approach, using a point source with magnitude 7.2 at ~17 km distance from Kalamata and considering rock site conditions, obtained an underestimated PGA value for the target site (0.145 g). Thus, the significance of considering both extended fault sources and site effects, as carried out in the approach here, is highlighted.

Seismic sources play an important role in the procedure. The faults employed for the presented scenarios have no association with historical earthquakes except for the Verga fault. Moreover, lack of paleoseismicity evidence obscures earthquake recurrence rates. For example, a Verga fault re-activation in an event similar to 1986 could be of low probability, since normal faults in Greece have recurrence intervals of hundreds, even thousands of years (e.g. Pantosti *et al.*, 2004; Chatzipetros *et al.*, 2005; Kokkalas *et al.*, 2007; Tsodoulos *et al.*, 2016; Koukouvelas *et al.*, 2017). Future availability of paleoseismicity data for the nearby faults would enable assigning a probability of occurrence for each scenario. Thereafter, we note the epistemic uncertainties included in the employed uniform sources extrapolated from empirical relations and field observations, in the absence of rupture histories.

The spatial variation in damage severity during the 1986 earthquake was attributed to soil conditions (e.g. Theodoulidis *et al.*, 2008) and to source and directivity effects due to the causative fault's proximity (Gariel *et al.*, 1991). To date, validation of the above implications has not been made possible, given that available data are aggregates for the whole town (Pomonis *et al.*, 2012). Our results indicate that both the soil response and the structures vulnerability have possibly contributed to the observed damage, given that: a) ambient noise HVSR peak frequencies were found to be similar to the eigenfrequencies of the majority of the existing building stock and to the recorded seismic excitations (Fig. 4), b) vulnerability of the affected buildings was high due to their age, c) the recordings of the 1986 earthquake at two neighbouring accelerometric stations (Fig. 5) having an interstation distance of ~300 m, show different characteristics, implying for site effects since the impact of differences of the source radiation pattern and the wave-path propagation should be negligible.

We question whether slight damage reported across the near-coast area, dominated by poor soil conditions has been due to site-induced de-amplification of seismic energy (EPPO, 1987). Taking into account that during that time low-rise unreinforced masonry constructions existed in the coastal area of Kalamata (Kazantzidou-Firtinidou *et al.*, 2016), we suggest that low

damage was the result of the response of the subsurface determined for periods >0.5 s, given that: a) such frequencies are favourable for medium-to-low height constructions prevailing in this city sector, and b) they lie away from the characteristic spectra of the strong ground motion (3-5 Hz, Fig. 4).

The damage in the harbour area of Kalamata was comparable to the respective damage in Aigion during the *Ms*=6.2 1995 earthquake, which was limited due to dampened ground motions in the soft and deep clayey deposits (Pomonis *et al.*, 2012). Similar to Kalamata, the buildings in the harbour were old and in a bad state, built without seismic resistance provisions (Athanassopoulos *et al.*, 1998). Interestingly, as in the case of Kalamata, ambient noise HVSR peak frequencies for much of the coastal area of Aigion were found <2 Hz (Kassaras and Kazantzidou-Firtinidou, 2015), a favourable value for the existing constructions. However, since no strong motion recordings are available for these sites, de-amplification of seismic excitations due to non-linear effects cannot be excluded.

The applied methodology resulted in a structural economic loss estimated in the order of 33 million Euros for an event similar to the one of 1986 (scenario A), an amount reduced by an order of 20 with respect to the 670 million Euros (GEM-ECD, 1986) cost of the real earthquake. We conclude that this is not an artefact but a favourable consequence of the structural interventions and the building of new constructions after the 1986 earthquake, demonstrating the necessity for modern codes and retrofitting/replacement of existing vulnerable structures.

The Xenokratis-Earthquakes was elaborated by the civil protection authorities of Kalamata in 2010, following the generic rules of Xenokratis Plan, taking into account only the arrangement of the urban fabric and the population, neglecting issues related to the structural seismic risk (Rigopoulou, 2013) which are highlighted by the current work. As a consequence, some anticipated emergency sheltering locations have been set up in areas of high risk, and hence might not be accessible or safe in case of a similar crisis to scenario B (Fig. 13B).

Eventually, seismic codes should continuously be updated according to the demands for a safe earthquake-structure interaction, leading to earthquake resilient cities, a representative example of which is Kalamata. Among the suggested options to improve the model outcome towards an effective implementation of risk treatment (ISO, 2009) are the rearrangement of vulnerability indices, the application of simplified mechanical methods [e.g. FEMA (2003), UE-LM2 by Milutinovic and Trendafilloski (2003)] and the update of damage functions.

9. Conclusions

The main outcomes of this study are summarized in the following points:
– both the soil and the structures have likely played important role in the 1986 damage distribution;
– the most hazardous part of Kalamata is the southern sector, capable of significantly amplifying seismic motions due to poor soil conditions, whereas the soil frequency response is found to be favourable for its constructions;
– the northern part of the city does not show significant amplification;
– synthetic seismic motions were found to exceed the effective PGA values of the seismic code;
– structural direct economic loss estimate for the most adverse scenario was found to be reduced by 20 times with respect to the 1986 earthquake costs;

– the emergency and civil protection Xenokratis-Earthquakes Plan elaborated by the Kalamata Municipality (KM, 2010) should be reconsidered with respect to the expected structural damage distribution, especially assuming the worst-case scenario.

This work, although open to improvements, may be considered worth integrating into a holistic seismic risk model for Kalamata by incorporating socioeconomic elements into the applied probabilistic methodology. The challenge is to stimulate improving the resilience of Greek cities against inherent seismic hazard.

REFERENCES

Anagnostopoulos S., Rinaldis D., Lekidis V., Margaris V. and Theodoulidis N.; 1987: *The Kalamata, Greece, earthquake of September 13, 1986.* Earthquake Spectra, **3**, 365-402.

Anderson J.G. and Hough S.E.; 1984: *A model for the shape of the Fourier spectrum of acceleration at high frequencies.* Bull. Seismol. Soc. Am., **74**, 1969-1993.

Ansal A., Erdik M., Studer J., Springman S., Laue J., Buchheister J., Giardini D., Faeh D. and Koksal D.; 2004: *Seismic microzonation for earthquake risk mitigation in Turkey.* In: Proc. 13th World Conf. Earthquake Eng., Vancouver, BC, Canada, Paper n. 1428.

Argyrakis K., Kountouris G. and Ioannidis K.; 1987: Damage assessment after the 1986 Kalamata earthquake. Report of working group for the Earthquake Plann. and Prot. Organiz. of Greece, Athens, Greece (in Greek).

ASPIDA: 2015: Infrastructure Upgrade for Seismic Protection of the Country and Strengthen Service Excellence through Action, project MIS-448326, implemented under the Action, Development Proposals for Research Bodies-ASPIS-KRIPIS (in Greek).

Athanassopoulos G.A., Pelekis P.C. and Leonidou E.A.; 1998: *Effects of surface topography and soil conditions on the seismic ground response - including liquefaction - in the Egion (Greece) 15/6/1995 earthquake.* In: Proc. 11th Eur. Conf. Earthquake Eng., Paris, France, 12 pp.

Beresnev I.A. and Atkinson G.M.; 1997: *Modeling finite-fault radiation from the ω² spectrum.* Bull. Seismol. Soc. Am., **87**, 67-84.

Bonnefoy-Claudet S., Cornou C., Bard P-Y., Cotton F., Moczo P., Kristek J. and Fah D.; 2006: *H/V ratio: a tool for site effects evaluation: results from 1D noise simulations.* Geophys. J. Int., **167**, 827-837.

Boore D.M.; 1983: *Stochastic simulation of high-frequency ground motions based on seismological models of the radiated spectra.* Bull. Seismol. Soc. Am., **73**, 1865-1894.

Boore D.M.; 2003: *Simulation of ground motion using the stochastic method.* Pure Appl. Geophys., **160**, 635-676.

Boore D.M.; 2009: *Comparing stochastic point-source and finite-source ground-motion simulations: SMSIM and EXSIM.* Bull. Seismol. Soc. Am., **99**, 3202-3216, doi:10.1785/0120090056.

Boukovalas G. and Sabatakakis N.; 1987: *Soil conditions and building damage in Kalamata from the 1986 earthquakes.* Bull. Publ. Works Res. Cent., Quarterly Scientific Review, **4**, 267-275, (in Greek with English abstract).

Brune J.N.; 1970: *Tectonic stress and spectra of seismic shear waves from earthquakes.* J. Geophys. Res., **75**, 4997-5009.

Calvi G.M., Pinho R., Magenes G., Bommer J., Restrepo-Velez L.F. and Crowley H.; 2006: *Development of seismic vulnerability assessment methodologies over the past 30 years.* ISET J. Earthquake Tech., **43**, 75-104.

CEN (European Committee for Standardization); 2002: *Eurocode 8: Design of structures for earthquake resistance, Draft No. 5.* CEN/TC250/SC8/N317, Brussels.

Chatzipetros A., Kokkalas S., Pavlides S. and Koukouvelas I.; 2005: *Palaeoseismic data and their implication for active deformation in Greece.* J. Geodyn., **40**, 170-188.

CLPW (Central Laboratory of Public Works); 1987: *Special publication on the geotechnical investigation in the frame of the microzonation study of Kalamata.* Bull. Publ. Works Res. Cent., Quarterly Scientific Review, **4**, 56 pp. (in Greek).

Dolce M., Kappos A., Masi A., Penelis G. and Vona M.; 2006: *Vulnerability assessment and earthquake damage scenarios of the building stock of Potenza (southern Italy) using Italian and Greek methodologies.* Eng. Struct., **28**, 357-371.

EAK2000; 2003: *Greek seismic code.* Earthquake Plann. and Prot. Organiz. (ed), Athens, Greece, 72 pp., 7 appendixes (in Greek).

EPANTYK; 2009: *Development of GIS software for the representation of the structural wealth of the municipalities of the country and of its structural vulnerability in buildings block level, YP.ES.A and H.D., KEDKE and HTC.* Earthquake Plann. and Prot. Organiz. (ed), Athens, Greece, 39 pp. (in Greek).

EPPO; 1987: *Microzonation study of Kalamata. Geology, neotectonic and geomorphological report.* Earthquake Plann. and Prot. Organiz. (ed), Athens, Greece, (in Greek).

FEMA (Federal Emergency Management Agency); 2003: *HAZUS-MH MR4. Technical manual.* Multi-hazard Loss Estimation Methodology, Earthquake Model. Department of Homeland Security, Washington, DC, USA, 712 pp.

Fountoulis I., Mariolakos I. and Ladas I.; 2014: *Quaternary basin sedimentation and geodynamics in SW Peloponnese (Greece) and late stage uplift of Taygetos Mt.* Boll. Geof. Teor. Appl., **55**, 303-324.

Ganas A. and Parsons T.; 2009: *Three-dimensional model of Hellenic Arc deformation and origin of the Cretan uplift.* J. Geophys. Res., **114**, B06404, doi:10.1029/2008JB005599.

Ganas A., Lekkas E., Kolligri M., Moshou A. and Makropoulos K.; 2012: *The 2011 Oichalia (SW Peloponnese, Greece) seismic swarm: geological and seismological evidence for E-W extension and reactivation of the NNW-SSE striking Siamo Fault.* Bull. Geol. Soc. Greece, **46**, 81-94.

Gariel J.-C., Bard P.Y. and Pitilakis K.; 1991: *A theoretical investigation of source, path and site effect during the 1986 Kalamata earthquake (Greece).* Geophys. J. Int., **104**, 165-177.

GEM-ECD (Global Earthquake Model - Earthquake Consequence Database); 1986: *Kalamata, Greece, 1986.* Pavia, Italy, <gemecd.org/event/18>.

Giovinazzi S. and Lagomarsino S.; 2004: *A macroseismic method for the vulnerability assessment of buildings.* In: Proc. 13th World Conf. Earthquake Eng., Vancouver, BC, Canada, Paper n. 896.

Grünthal G. (ed); 1998: *European Macroseismic Scale 1998.* Cahiers du Centre Européen de Géodynamique et de Séismologie, Luxembourg, Vol. 15, 99 pp.

HTC (Hellenic Technical Chamber); 2014: Lessons learned from the earthquakes in Cephalonia, Thessaloniki, Greece, 489: 4, (in Greek).

Herak M.; 2008: *ModelHVSR: a Matlab® tool to model horizontal-to-vertical spectral ratio of ambient noise.* Comput. Geosci., **34**, 1514-1526.

ISO (International Organization for Standardization); 2009: *IEC31010, Risk management - Risk assessment techniques.* ISO Central Secretariat, Geneva, Switzerland, 176 pp.

Kalteziotis N., Sambatakakis N. and Vasileiou I.; 1992: *Assessment of the dynamic characteristics of soils in Greece.* In: Proc. 2nd Pan-Hellenic Congr. Geotech. Eng., Thessaloniki, Greece, Vol. 2, pp. 239-246.

Kappos A.J. and Dimitrakopoulos E.G.; 2008: *Feasibility of pre-earthquake strengthening of buildings based on cost-benefit and life-cycle cost analysis, with the aid of fragility curves.* Nat. Hazards, **45**, 33-54.

Karantoni F., Pantazopoulou S. and Ganas A.; 2017: *Confined masonry as practical seismic construction alternative-the experience from the 2014 Cephalonia Earthquake.* Front. Struct. Civ. Eng., doi:10.1007/s11709-017-0390-1.

Kashima T.; 2007: *ViewWave, a viewer for strong motion records.* Building Res. Inst., Tsukuba, Japan, <iisee.kenken.go.jp/staff/kashima/viewwave.html>.

Kassaras I. and Kazantzidou-Firtinidou D.; 2015: *Scenarios of risk assessment in the built environment of Aegion.* ASPIDA, Technical Report, 101 pp., (in Greek, unpublished).

Kassaras I. and Kazantzidou-Firtinidou D.; 2017: *Environmental hazards methodologies for risk assessment and management.* In: Dalezios N. (ed), Water Intelligence Online, IWA Publishing, Vol. 16, doi:10.2166/9781780407135.

Kassaras I., Kalantoni D., Kouskouna V., Pomonis A., Michalaki K., Stoumpos P., Mourloukos S., Birmpilopoulos S. and Makropoulos K.; 2014: *Correlation between damage distribution and soil characteristics deduced from ambient vibrations in the old town of Lefkada (W Greece).* In: Proc. 2nd Eur. Conf. Earthquake Eng. Seismol., Istanbul, Turkey, Paper n. 251.

Kassaras I., Kalantoni D., Benetatos C., Kaviris G., Michalaki K., Sakellariou N. and Makropoulos K.; 2015: *Seismic damage scenarios in Lefkas old town (W Greece).* Bull. Earthquake Eng., **13**, 3669-3711, doi:10.1007/s10518-015-9789-z.

Kassaras I., Kapetanidis V. and Karakonstantis A.; 2016: *Seismicity and 3D tectonic stress field distribution in the western Hellenic Arc.* In: Extended Abstract 35th Gen. Assoc. Eur. Seismol. Commission, Trieste, Italy, n. ESC2016-605-2.

Kassaras I., Papadimitriou P., Kapetanidis V. and Voulgaris N.; 2017: *Seismic site characterization at the western*

Cephalonia Island in the aftermath of the 2014 earthquake series. Int. J. Geo-Eng., **8**, 1-22, doi:10.1186/s40703-017-0045-z.

Kazantzidou-Firtinidou D., Kassaras I., Ganas A., Tsimi C., Sakellariou N., Mourloukos S., Stoumpos P., Michalaki K. and Giannaraki G.; 2016: *Seismic damage scenarios in Kalamata (S. Greece)*. Bull. Geol. Soc. Greece, **50**, 1495-1505, doi:10.12681/bgsg.11862.

KM (Kalamata Municipality); 2010: (http://www.kalamata.gr/images/arthra/2017/03/07-11548/PolitikhProstasia_Xarths.pdf), last accessed 30/11/2017.

Kokkalas S., Pavlides S., Koukouvelas I., Ganas A. and Stamatopoulos L.; 2007: *Paleoseismicity of the Kaparelli Fault (eastern Corinth Gulf): evidence for earthquake recurrence and fault behaviour*. Boll. Soc. Geol. It., **126**, 387-395.

Konno K. and Ohmachi T.; 1998: *Ground-motion characteristics estimated from spectral ratio between horizontal and vertical components of microtremor*. Bull. Seismol. Soc. Am., **88**, 228-241.

Koukouvelas I.K., Zygouri V., Papadopoulos G.A. and Verroios S.; 2017: *Holocene record of slip-predictable earthquakes on the Kechreai Fault, Gulf of Corinth, Greece* J. Struct. Geol., **94**, 258-274.

Kouskouna V. and Kaviris G.; 2014: *Seismic hazard study in Messinia (SW Peloponnese) area.* In: Proc. 2nd Eur. Conf. Earthquake Eng. Seismol., Istanbul, Turkey, doi:10.13140/2.1.2196.4168.

Ktenidou O.-J., Gélis C. and Bonilla L.F.; 2015: *A study on the variability of Kappa (κ) in a borehole: implications of the computation process.* Bull. Seismol. Soc. Am., **103**, 1048-1068, doi:10.1785/0120120093.

Laigle M., Sachpazi M. and Hirn A.; 2004: *Variation of seismic coupling with slab detachment and upper plate structure along the western Hellenic subduction*. Tectonophys., **391**, 85-95.

Leventakis G.A., Lekidis V., Papaioannou Ch., Zacharopoulos S., Tsokas G. and Kiratzi A.; 1992: *Equal-Intensity contour map for the city of Kalamata due to September 1986 earthquake.* In: Proc. 1st Hellenic Conf. Earthquake Eng. and Eng. Seismol., Athens, Greece, Vol. 2, pp. 321-330, (in Greek).

Lotzetidis K.D., Anastasiadis A. and Raptakis D.; 1992: *Relations for correlation between VS - NSPT for soils in Greece.* In: Proc. 2nd Pan-Hellenic Congress Geotech. Eng., Thessaloniki, Greece, pp. 419-425.

Lyon-Caen H., Armijo R., Drakopoulos J., Baskoutass J., Delibassis N., Gaulon R., Kouskouna V., Latousakis J., Makropoulos K., Papadimitriou P., Panastasiou D. and Pedotti G.; 1988: *The 1986 Kalamata (south Peloponnesus) Earthquake: detailed study of a normal fault, evidences for east-west extension in the Hellenic arc*. J. Geophys. Res., **93**, 14967-15000.

Makropoulos K., Kaviris G. and Kouskouna V.; 2012: *An updated and extended earthquake catalogue for Greece and adjacent areas since 1900.* Nat. Hazards Earth Syst. Sci., **12**, 1425-1430.

Margaris B.N. and Boore D.M.; 1998: *Determination of Δσ and κ₀ from response spectra of large earthquakes in Greece.* Bull. Seismol. Soc. Am.*,* **88**, 170-182.

Margaris B.N. and Hatzidimitriou P.M.; 2002: *Source spectral scaling and stress release estimates using strong-motion records in Greece.* Bull. Seismol. Soc. Am., **92**, 1040-1059.

McGuire R.K.; 2001: *Deterministic vs. probabilistic earthquake hazards and risks.* Soil Dyn. Earthquake Eng., **21**, 377-384.

Milutinovic Z. and Trendafiloski G.; 2003: *An advanced approach to earthquake risk scenarios with applications to different European towns - Risk-UE.* European Commission, Brussels, Belgium, WP4, Vulnerability of current buildings, Project EVK4-CT-2000-00014, 10 pp.

Motazedian D. and Atkinson G.M.; 2005: *Stochastic finite fault modeling based on a dynamic corner frequency.* Bull. Seismol. Soc. Am., **95**, 995-1010.

Nakamura Y.; 1989: *A method for dynamic characteristics estimation of subsurface using microtremor on the ground surface.* Railway Tech. Res. Inst., **30**, 25-33.

Nakamura Y.; 2000: *Clear identification of fundamental idea of Nakamura's technique and its applications.* In: Proc. 12th World Conf. Earthquake Eng., Auckland, New Zealand, Paper n. 2656.

Nakamura Y.; 2008: *On the H/V spectrum,* In: Proc. 14th World Conf. Earthquake Eng., Beijing, China, 10 pp.

Panou A., Theodoulidis N., Hatzidimitriou P., Stylianidis K. and Papazachos C.; 2005: *Ambient noise horizontal-to-vertical spectral ratio in site effects estimation and correlation with seismic damage distribution in urban environment: the case of the city of Thessaloniki (northern Greece).* Soil Dyn. Earthquake Eng., **25**, 261-274.

Pantosti D., De Martini P.M., Papanastassiou D., Lemeille F., Palyvos N. and Stavrakakis G.; 2004: *Paleoseismological trenching across the Atalanti Fault (central Greece): evidence for the ancestors of the 1894 earthquake during the middle ages and Roman times.* Bull. Seismol. Soc. Am., **94**, 531-549.

Papazachos B. and Papazachou C.; 2003: *The earthquakes of Greece, 3rd ed.* Ziti Publ., Thessaloniki, Greece, 286 pp.

Papazachos B.C., Papaioannou C.A., Margaris B.N. and Theodulidis N.P.; 1993: *Regionalization of seismic hazard in Greece based on seismic sources.* Nat. Hazards, **8**, 1-18.

Papazachos B., Karakostas V., Papazachos C. and Scordilis E.; 2000: *The geometry of the Wadati-Benioff zone and lithospheric kinematics in the Hellenic Arc.* Tectonophys., **319**, 275-300.

Pitilakis K., Riga E. and Anastasiadis A.; 2012: *Design spectra and amplification factors for Eurocode 8.* Bull. Earthquake Eng., **10**, 1377-1400.

Pomonis A., Gaspari M. and Karababa F.S.; 2012: *Seismic vulnerability assessment for buildings in Greece based on observed damage data sets.* Boll. Geof. Teor. Appl., **55**, 501-534.

Rigopoulou D.; 2013: *Study and validation of the "Xenokratis-Earthquakes" plan and proposals for Kalamata.* MSc Dissertation, Charokopeio University, Dept. of Geography, Kallithea, Grecia, 134 pp. (in Greek).

Rodriguez V.H.S. and Midorikawa S.; 2002: *Applicability of the H/V spectral ratio of microtremors in assessing site effects on seismic motion.* Earthquake Eng. Struct. Dyn., **31**, 261-279.

Roumelioti Z., Kiratzi A., Margaris B. and Chatzipetros A.; 2017: *Simulation of strong ground motion on near-fault rock outcrop for engineering purposes: the case of the city of Xanthi (northern Greece).* Bull. Earthquake Eng., **15**, 25-49, doi:10.1007/s10518-016-9949-9.

SESAME; 2004: *Guidelines for the implementation of the H/V spectral ratio technique on ambient vibrations - measurements, processing and interpretations.* European Commission, Brussels, Belgium, WP12, Deliverable D23.12, Project EVG1-CT-2000-00026, 62 pp.

Sibson R.; 1981: *A brief description of natural neighbour interpolation.* In: Barnett V. (ed), Vic, Interpreting multivariate data, Wiley, Chichester, NY, USA, pp. 21-35.

Slejko D., Santulin M. and Garcia J.; 2014: *Seismic hazard estimates for the area of Pylos and surrounding region (SW Peloponnese) for seismic and tsunami risk assessment.* Boll. Geof. Teor. Appl., **55**, 433-468.

Theodoulidis N., Cultrera G., Tento A., Faeh D., Atakan K., Bard P-Y., Panou A. and the SESAME Team; 2004: *Empirical evaluation of the horizontal to vertical spectral ratio technique: results from the SESAME Project.* In: Proc. 13th World Conf. Earthquake Eng., Vancouver, BC, Canada, Paper n. 2323.

Theodoulidis N., Cultrera G., De Rubeis V., Cara F., Panou A., Pagani M. and Teves-Costa P.; 2008: *Correlation between damage distribution and ambient noise H/V spectral ratio: the SESAME project results.* Bull. Earthquake Eng., **6**, 109-140.

Theofanopoulos N. and Dan K.; 1988: *Simulation of the ground motion at Kalamata city - Greece.* In: Proc. 9th World Conf. Earthquake Eng., Tokyo-Kyoto, Japan, Vol. 2, pp. 837-842.

Tselentis G. and Danciu L.; 2008: *Empirical relationships between Modified Mercalli Intensity and engineering ground-motion parameters in Greece.* Bull. Seismol. Soc. Am., **98**, 1863-1875.

Tsiambaos G. and Sabatakakis N.; 2011: *Empirical estimation of shear wave velocity from in situ tests on soil formations in Greece.* Bull. Eng. Geol. Environ., **70**, 291-297.

Tsodoulos I.M., Stamoulis K., Caputo R., Koukouvelas I., Chatzipetros A., Pavlides S., Gallousi C., Papachristodoulou C. and Ioannides K.; 2016: *Middle-Late Holocene earthquake history of the Gyrtoni Fault, central Greece: insight from optically stimulated luminescence (OSL) dating and paleoseismology.* Tectonophys., **687**, 14-27.

Valkaniotis S., Betzelou K., Zygouri V., Koukouvelas I. and Ganas A.; 2015: *Late Quaternary tectonic activity and paleoseismicity of the eastern Messinia Fault Zone, SW Peloponessus (Messinia, Greece).* In: Abstracts EGU General Assembly Conf., Wien, Austria, Vol. 17, n. 13215.

Wells D.L. and Coppersmith K.J.; 1994: *New empirical relationships among magnitude, rupture length, rupture width, rupture area and surface displacement.* Bull. Seismol. Soc. Am., **84**, 974-1002.

Wyss M. and Rosset P.; 2013: *Mapping seismic risk: the current crisis.* Nat. Hazards, **68**, 49-52, doi:10.1007/s11069-012-0256-8.

Xenokratis-Earthquakes Plan; 2003: *Ministerial Decision 1299.* Government Paper Sheet 423B.

Zygouri V., Valkaniotis S., Betzelou K., Ganas A. and Koukouvelas I.; 2015: *Paleoseismicity of the eastern Messinia Fault Zone, SW Peloponnesus (Messinia, Greece).* In: Abstracts 2015 Geol. Soc. Greece Ann. Sci. Meeting, Athens, Greece, p. 51.

Corresponding author: Ioannis Kassaras
Dept. of Geophysics-Geothermics, Faculty of Geology and Geoenvironment, National and Kapodistrian University of Athens
Panepistimiopolis, Athens 15784, Greece
Phone: +30 2107274792; e-mail: kassaras@geol.uoa.gr